Fault detection for parallel operating machines

Dustin Helm
Laurentian University, Sudbury, Canada, and
Markus Timusk
Bharti School of Engineering, Laurentian University, Sudbury, Canada

Received 24 October 2018
Revised 23 February 2019
Accepted 20 March 2019

Abstract

Purpose – The purpose of this paper is to demonstrate that by utilizing the relationship between redundant hardware components, inherent in parallel machinery, vibration-based fault detection methods can be made more robust to changes in operational conditions. This work reports on a study of fault detection on bearings operating in two parallel subsystems that experience identical changes in speed and load.

Design/methodology/approach – This study was carried out using two identical subsystems that operate on the same duty cycle. The systems were run with both healthy and a variety of common bearing faults. The faults were detected by analyzing the residual between the features of the two vibration signatures from the two subsystems.

Findings – This work found that by utilizing this relationship in parallel operating machinery the fault detection process can be improved. The study looked at several different types of feature vector and found that, in this case, features based on envelope analysis or autoregressive model work the best, whereas basic statistical features did not work as well.

Originality/value – The proposed method can be a computationally efficient and simple solution to monitoring non-stationary machinery where there is hardware redundancy present. This method is shown to have some advantages over non-parallel approaches.

Keywords Condition monitoring, Vibration analysis, Fault detection

Paper type Research paper

1. Introduction

Condition monitoring techniques for rolling-element bearings generally involve the measurement and interpretation of some parameter that can inform the condition of the machine. Typically, these methods require extraction of features that are able to indicate changes in mechanical condition (i.e. a fault) while at the same time are not sensitive to normal changes that are not related to mechanical condition (such as speed, load, ambient temperature, age of component, etc.). These techniques require the collection of sensor data to determine a baseline operating conditions to which new data from unknown classes can be compared. To be effective, these approaches depend on the presumption that changes in the sensor data (revealed by comparison with the baseline) are due to mechanical changes in the machine (i.e. fault). Most approaches to fault detection rely on signal processing techniques to extract elements of the signal that are likely to display fault signatures. Changes in speed and load, as well as other changes in the machines operating conditions, can have an effect on the raw signal that obscures the minor changes associated with a fault condition (Zimroz *et al.*, 2014). This has various effects on the features and feature extraction process and can be seen in the change in bearing defect frequencies with respect to the bearings rotational speed (McBain and Timusk, 2009). Monitoring variable speed machinery becomes difficult due to the interaction between angle, and time dependent characteristics (Abboud *et al.*, 2015). Some current approaches to the monitoring of non-stationary machinery include signal processing techniques such as order tracking, time-frequency domain analysis and cyclo-non-stationary signal analysis (Uma Maheswari and Umamaheswari, 2017; Zhao and Wang, 2011; Law *et al.*, 2012; Prudhom *et al.*, 2017; Abboud *et al.*, 2017) as well as machine learning algorithms that look for patterns in the data that are the result of changes in condition(Goreczka and Strackeljan, 2012; Wang and Kanneg, 2009). Solutions to

Journal of Quality in Maintenance Engineering
Vol. 26 No. 2, 2020
pp. 335-348

1355-2511
DOI 10.1108/JQME-10-2018-0087

monitoring non-stationary machinery typically rely on extensive training data sets that attempt to cover the entire machine operating window, as well as *a priori* information about the failure signature. Similar to the effects of speed and load changes, normal wear and environmental factors (i.e. ambient temperature) can also have a transient effect on the raw data leading to similar problems as with non-stationary machinery.

Another well-known technique for detection of faults in systems is analytical redundancy. This is defined as the use of at least two ways to determine a variable, one of which is in the form a mathematical model (Isermann and Ballé, 1997). So called analytical redundancy relations (ARRs) can be used to generate residuals between measured sensor values and the mathematical model. The number of ARRs that can be used is equal to the number of sensors for the system. The models can come in the form of process models or signal models (Isermann, 2006). The generated residuals between the model and measured values can take several forms to aid in fault isolation. They can be: diagonal residuals where each element in a residual represents one fault, directional residuals where each fault generates a straight line in the residual space and structured residuals where each residual responds to a subset of possible faults and it setup such that the fault type can always be isolated (Gertler, 1997). These residuals can be found several different ways including by using party relations which is presented by Gertler (1997). ARRs which were originally developed for linear systems were extended to non-linear systems by Staroswiecki and Comtet-Varga (2001). More recently, Willersrud *et al.* (2015) used ARRs to detect incidents during drilling for the oil and gas industry. ARRs were also proposed as a solution to fault detection and isolation as part of larger fault accommodation scheme for quadruped robots in the study of Gor *et al.* (2018). In the aforementioned work, ARRs were used to detect failures in actuators so that a fault tolerant control system could be implemented.

Hardware redundancy is an important tool for fault tolerant design that can also be implemented to aid in fault detection schemes. Hardware redundancy is the inclusion of multiple redundant components to build fault tolerance and increase reliability. Hardware redundancy is commonly used for sensor fault accommodation (Gor *et al.*, 2018; Medjaher *et al.*, 2006). Hardware redundancy when implemented for mechanical systems often consists of multiple components operating in parallel, and the failure of one results in increased load on the other components (Isermann, 2006).

This work introduces a non-model-based statistical approach that builds on the work done with analytical redundancy methods, except that the analytical system model is replaced with a real physical system. It is referred to here as experimental feature residual analysis and it applies to a specific class of machinery, described here as connected parallel machinery. Connected parallel machinery is defined as a strict hardware redundancy where each of the identical mechanical subsystems shares a forcing function and operating conditions. They can be linked, either mechanically or through a control system forcing them to follow the same speed and load changes. Some examples of connected parallel machinery could be pumps or generators setup in a parallel arrangement, gearbox bearings attached to the same shaft or even jet engines on twin engine aircraft.

This class of machinery can present a unique opportunity for condition monitoring systems due to the ability to gain reference information about any non-stationary non-fault-related signal elements from redundant mechanical systems. Rather than comparing new data to historical baseline data, this technique compares new data to new data from the parallel systems in real time. Preliminary work in this area has shown some promise in being able to detect faults in non-stationary machinery without the use of fault data for training. This method has already been shown to work on parallel operating gear pumps (Rose *et al.*, 2016) as well as on idler pulley bearings in the studies of Helm *et al.* (2016) and Helm and Timusk (2017).This work will extend that presented in the study of Helm and Timusk (2017) to include analysis of multiple different possible feature vectors, as well as to

include analysis of the performance difference when compared to a similar non-parallel system. It should be noted here that when the identical components operate under the same conditions (described here as connected parallel machinery) their failures are highly unlikely to occur at the same time. In fact, for a group of 30 or more identical bearings the difference in life between the longest and shortest can be as much as 20 times (Zaretsky, 2013). Another key factor in the usefulness of the proposed method is its sensitivity to system uncertainties such as manufacturing tolerances. While in the theoretical ideal case where two components are completely identical and operate in the exact same conditions it seems to be a trivial task to generate a residual that will be sensitive to the presence of a fault (since when healthy the two vibration signal would be strictly identical). However, for real machinery this is not the case, there are many uncertainties that will have a small effect on the individual vibration signals. In this work it will be shown that the proposed method is capable of detecting faults in the presence of these unavoidable uncertainties.

The main contribution of this work is that by analyzing components in parallel rather than as separate systems it is possible to gain significant advantages for fault detection. This manuscript first goes into detail about the proposed method explaining the necessary steps and outlines well-known and robust measures that can be implemented with this technique. Next, the parallel machinery simulator that was used to test two mechanical subsystems is described. Finally, results for the detection of a number of different faulted bearings using both a parallel and non-parallel method are presented and summarized.

2. Methodology

2.1 Experimental feature residual analysis

Experimental feature residual analysis is an approach for condition monitoring of parallel systems that capitalizes on the configuration of parallel machinery to detect incipient faults in non-stationary machinery that was first introduced in the study of Helm and Timusk (2017). The general architecture for detecting faults in parallel systems through residual analysis is shown in Figure 1. The approach requires simultaneous data collection on the two observed parallel subsystems using identical transducers that are identically mounted. Similar to non-parallel approaches to fault detection, in experimental feature residual analysis, raw data from each subsystem is first segmented and then features are extracted from each segment. It is after feature extraction that the residual value between the subsystems is calculated. This residual is then used similar to a novelty score in a one class classification system to determine the likelihood of the presence of a fault. Using this technique, transient elements (such as those due to speed and load changes or changes in environmental or normal wear conditions) of the measured parameter can be canceled out from the system because they will be the same in both parallel subsystems. A drawback of this system is that in reducing the data from the two parallel subsystems into one residual value information about the location of the fault (which subsystem) or type of fault is lost. However, this can be negated in situations where there are more than two subsystems.

The raw vibration signals were segmented into short-time segments that were analyzed separately. The segment length was ten shaft revolutions. This was selected such that each segment contains several repetitions of any signal events phase locked to the shaft frequency, while is also short enough that each segment contains only a small window of the machines operating conditions. Each segment was also windowed using a Hanning window to reduce any leakage errors. The segments were also overlapped by 50 percent to eliminate losses due to the windowing process.

Features were then extracted from each segment that could adequately describe the important information contained within the raw signal. It is generally desirable have features that will be sensitive to the fault without being too sensitive to speed and load changes in the machine. In this work, it is still desirable to have features that will be the

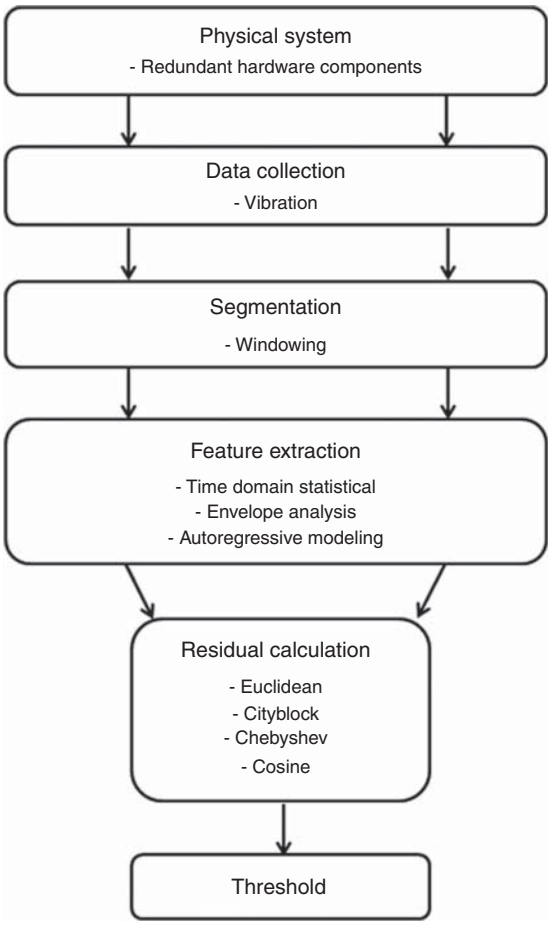

Figure 1.
Experimental feature residual analysis applied to REBs

most sensitive to fault condition, however, it was less affected by other influences on the signal due to the parallel setup. In this work, three different feature vectors are considered with varying degrees of complexity, they are described in Section 2.3.

After feature extraction a metric that quantifies the residual value for the machine was calculated. This score indicates the likelihood that fault is present in either subsystem. This can be done by evaluating the difference between the parallel feature vectors. This process reduces the information from the two feature vectors to a single number to which a threshold can be applied in order to determine if a fault is present. This measurement of the difference can be done in a number a ways but most simply is measurement of the distance between the two vectors, see Section 2.2. During the distance measurement process the difference between individual elements in the two feature vectors are normalized between −1 and 1 to ensure equal weighting between all the features in the final value.

2.2 Distance metrics employed for residual calculation

To calculate the residual values between feature vectors, several distance metrics were employed to quantify the difference between the multi-dimensional feature vectors. The distance metrics

used in the research to measure the overall difference between feature vectors were: Euclidean, City block, Chebyshev (special cases of the Minkowski metric where $p = 2$, 1 and ∞, respectively) and Cosine. The equations for which are listed in Table I.

2.3 Feature extraction

2.3.1 Time domain statistics. The first feature vector used consisted of simple time domain statistics features. Five different features were calculated using the raw, time domain signal as well as the signal after applying two different bandpass filters (15 features total). The bandpass filters were used to obtain values more descriptive the higher frequency components of the signal because the raw data were dominated by gear mesh frequencies. The features used were RMS, Kurtosis, standard deviation crest factor and skewness. These features are typical statistical features used for bearing condition monitoring (Jiang *et al.*, 2014). Note that the frequency bands in this instance were the raw signal, 3,500–4,900 Hz and 2,500–3,500 Hz.

2.3.2 Autoregressive feature extraction. Autoregressive models are often used to characterize signals as can provide a compact representation of a complicated signal (Hoell and Omenzetter, 2016). An AR model that takes the form of Equation (1) is calculated to represent the raw data. This model can be found using a linear least squares method that seeks to minimize the total error between the model output and the real data:

$$y(n) = b_0 x(n) + a_1 y(n-1) + a_2 y(n-2) \cdots a_p y(n-p). \quad (1)$$

After the model is generated for a given segment, the coefficients (a_1–a_p) become the signal features. It has been shown that these coefficients are sensitive to the health state of a machine (Timusk *et al.*, 2008; Cong *et al.*, 2012). The order of the model determines the number of elements in the feature vector and can be optimized using Akaike information criterion (Wang and Makis, 2009; Figueiredo *et al.*, 2011). In this work, AR models of order 10 were used.

2.3.3 Envelope analysis. The method here is adapted from the method presented in the study of Randall and Antoni (2011) to be used for a parallel application. This method and the parallel version presented here will serve as a basis for comparing the performance of parallel vs non-parallel in non-stationary applications.

First, linear prediction is used to remove deterministic frequencies that are shared between the signals from both subsystems. Linear prediction has been used successfully for noise elimination (Samy and Bassiuny, 2016; Assaad *et al.*, 2014), however, it is typically

Name	Equation	Description
Euclidean	$\sqrt{\sum_{i=1}^{k}\left(\frac{L_i - R_i - m_i}{n_i}\right)^2}$	Straight line distance in normalized feature space
City block	$\sum_{i=1}^{k} abs\left(\frac{L_i - R_i - m_i}{n_i}\right)$	Distance following feature directions only. Less sensitive to high individual values than Euclidean
Chebyshev	$\max\left(\frac{L_i - R_i - m_i}{n_i}\right)$	Max distance along any one feature. Most sensitive to high individual values
Cosine	$1 - \frac{LR'}{\sqrt{(LL')(RR')}}$	Cosine of the angle between feature vectors

Notes: L and R are the k dimensional feature vectors from either subsystem (left and right subsystem) and m_i and n_i are the normalization factors (mean and standard deviation of healthy data) for the difference in the ith feature. For the Euclidean, City block and Chebyshev distances, the features were normalized after subtracting, as described in Section 2.1, however, for the cosine distance this was not possible so the features were normalized separately, prior to calculating the distance.

Table I.
Distance metrics

applied using a single signal eliminating frequencies from itself. In this work, we look to take advantage of the parallel aspect of the signals and eliminate only the shared deterministic elements from each signal. This is done by systematically creating a linear prediction model for each signal segment, then using that model to remove frequencies from the corresponding (i.e. same time period) segment of the other signal. The frequencies are removed by continuously predicting the next value in the signal using the history of the original signal and the corresponding model weights (see Equation (2)). The new signal then becomes the difference between the original value and the predicted value. Since the models are updated for every segment and used for segments during the same time interval it is expected that this method will respond quickly to changes in this signal:

$$y(n) = \sum_{i=0}^{l} b_i \times x_{l-i}. \tag{2}$$

The model weights $b(i)$ for the linear prediction FIR filter are found using the Yule–Walker equations, solved by the Levinson–Durbin algorithm. This is discussed further in the study of Kay and Marple (1981).

After the deterministic frequencies were removed, minimum entropy deconvolution (MED) was employed to reduce the effects of the signal transfer path. MED, first proposed by R. Wiggins (1978), has been successfully implemented in many applications including gear and bearing fault detection (Sawalhi *et al.*, 2007). This is achieved by assuming the original signal is impulsive, and searching for the filter that will minimize the entropy of the signal (Barszcz and Sawalhi, 2012). This filter can be found using several methods, for a review see McDonald *et al.* (2012).

Envelope analysis was then preformed on the resulting signals using the Hilbert technique (Randall, 2004a, b). To summarize this technique, first, the complex Fourier spectrum of the signal band is taken and a frequency band of which to obtain the envelope is selected. This band is then shifted to zero and padded with zeros to double the length. The inverse transform is then taken to obtain the analytic signal, from which the envelope can be obtained by calculating its amplitude. After the envelope signal is obtained, fault sensitive features are extracted from the amplitude spectrum of the envelope signals. These features are listed in Table II.

Name	Equation	Frequency band	Description
Spectral difference	$\frac{\sum_{i=1}^{l}\sqrt{(a1(i)+a2(i))\times\lvert a1(i)-a2(i)\rvert}}{l}$	3,900–4,900 hz	Measure of the total difference between amplitude spectra of the 2 envelope signals
Outer race fault frequency	$\frac{a1(f_o)-a2(f_o)}{\text{minimum}(\text{mean}(a1),\text{mean}(a2))}$	2,500–2,900 hz 3,900–4,900hz	Relative difference amplitude at the outer race fault frequency (f_o) (calculated from average speed for the segment)
Inner race fault frequency	$\frac{a1(f_i)-a2(f_i)}{\text{minimum}(\text{mean}(a1),\text{mean}(a2))}$	2,500–2,900 hz 3,900–4,900 hz	Relative difference amplitude at the inner race fault frequency (f_i) (calculated from average speed for the segment)
Rolling-element fault frequency	$\frac{a1(f_r)-a2(f_r)}{\text{minimum}(\text{mean}(a1),\text{mean}(a2))}$	2,500–2,900 hz 3,900–4,900 hz	Relative difference amplitude at the inner race fault frequency (f_r) (calculated from average speed for the segment)
Pulley frequency	$\frac{a1(f_p)-a2(f_p)}{\text{minimum}(\text{mean}(a1),\text{mean}(a2))}$	2,500–2,900 hz 3,900–4,900 hz	Relative difference amplitude at the inner race fault frequency (f_p) (calculated from average speed for the segment)

Note: $a1$ and $a2$ are the amplitude spectra of the squared envelope of each signal

Table II.
Frequency domain features

The spectral difference feature was not used for the 2,500–2,900 hz signal band because it was dominated by a modulation at the frequency of the gear pumps, making these measurements inconsistent. However, the specific values for the fault frequencies did provide significant information.

3. Experimental setup

3.1 Parallel machinery simulator

The experiments for this work were carried out using a machine refereed to here as the parallel machinery simulator. It consists of two identical subsystems that are both loaded and driven in a parallel manner. The subsystems are each driven by a 10 hp induction motor and they are loaded hydraulically using gear pumps that pump through a common manifold. The pressure in the manifold can be controlled using a solenoid actuated proportional valve. Power is transmitted from the motors to the pumps through a gearbox with a 3:1 reduction and a serpentine belt drive system similar to that of an automotive accessory drive, see Figure 2. Additional detail about the control strategy and system employed is described in McBain *et al.*'s (2013) study.

The parallel machinery simulator is instrumented with several different types of sensors, including pressure sensors, accelerometers encoders and acoustic emissions sensors. The signals from all the sensors with the exception of the encoder are read directly into the LabVIEW control program to be recorded and/or used to control the machine. The encoder signal is, first, run through the motor controller that is used to control the motor speed. The manifold pressure is controlled using a solenoid actuated proportional valve, which is driven by a proportional driver that is controlled using the control program. Varying the manifold pressure controls the loads seen through the system.

3.2 Duty cycle

The duty cycle used for these tests was defined to include all combinations of three different discrete levels of steady state speed and load as well as continuously varying run up/run down conditions (see Figure 3). The maximum speed the system reaches is 600 rpm at the motor and the maximum load corresponds to 550 lbf acting radially on the bearings that were tested.

3.3 Faulted components and data collection

The components that were tested in this work were the bearings inside the idler pulley on the belt drive system (see Figure 4). The idler pulley is located between the load pulley and the drive pulley on the tension side of the system; due to this the radial load on the bearing corresponds directly with the load applied at the pump.

Before the bearings were properly assembled by the manufacture, mechanical faults were introduced to their contact surfaces using electrical discharge machining. The types of

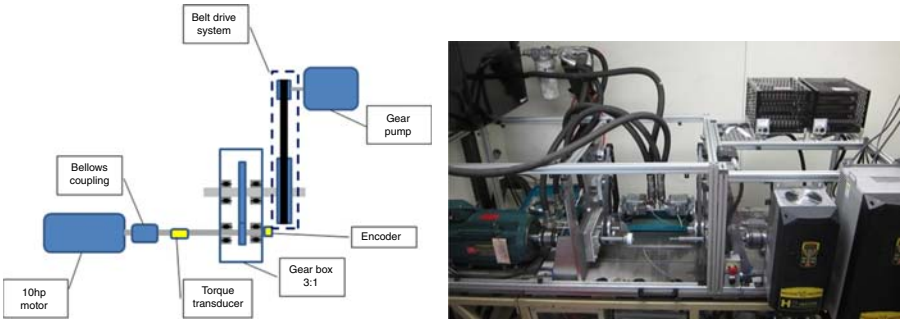

Figure 2.
Parallel machinery simulator

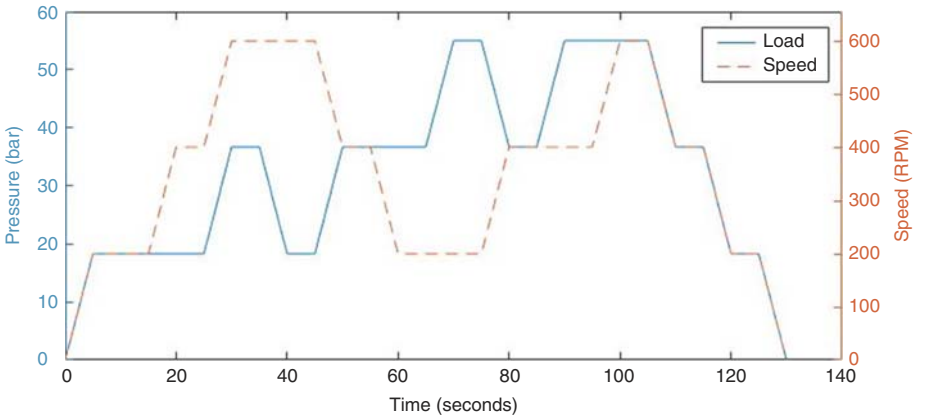

Figure 3.
Duty cycle

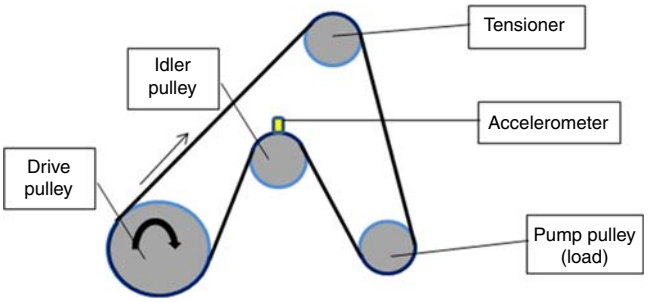

Figure 4.
Belt drive system diagram

faults created were outer race, inner race and rolling-element faults and ranged in size from 1.5 mm to 0.25 mm, see Plate 1. All of the inner and outer race faults are 0.1 mm deep and span 2 mm across the bearing races. The rolling-element faults are also 0.1 mm deep; however, they are square with a size corresponding to the listed fault size. Each faulted bearing was tested in both of the machine subsystems. Eight different healthy bearings were also used to both run opposite the faulted bearings and for healthy tests (no fault in either subsystem). In total, there were 8t tests with a healthy condition and 30 tests with a fault (two for each fault condition). Each test constitutes one run through the duty cycle

Plate 1.
Idler pulley bearing with 1.5 mm outer race fault

depicted in Section 3.2. The accelerometers were mounted to the post that supports the idler pulley in a direction aligned with the load direction on the pulley. These raw data were collected using a sampling rate of 10 KHz.

4. Results

4.1 Parallel vs non-parallel, non-stationary results

The results below illustrate the percent of segment distance measurements above a set threshold for all healthy tests, fault types and sizes. The results were calculated using all four distance metrics and all three feature vector types described in Sections 3.2 and 3.3, respectively. For the non-parallel results presented here, the distance measurement given is a measurement to a feature vector representing the average values for a healthy system. The thresholds were chosen to achieve an average of approximately 10 percent above the threshold for the healthy tests.

4.1.1 Time domain statistics. As can be seen in Table III, using the time domain statistics features this method was able to produce a significant increase in the number of distance measurements above the predetermined threshold for both the inner and outer race faults, while the healthy tests remained within a reasonable distance from the 10 percent target. However, the rolling-element fault did not produce significant results. Moreover, the parallel method performed similar or better than the non-parallel version. Notably, the inner race fault detection showed significant improvement and the deviation for the healthy test is reduced (see test 1 for the healthy non-parallel results). Also, note that the Euclidean and Chebyshev distances preform the best for most situation and cosine distance preforms the worst.

4.1.2 Autoregressive features. As can be seen in Table IV, using AR features in place of the time domain statistic features improves the results of the parallel method significantly, whereas the results for the non-parallel approach seem to have become less consistent. In the case of using the AR features, the parallel method has greatly improved the classification results.

Healthy

	Parallel								Non-parallel							
Test number	1	2	3	4	5	6	7	8	1	2	3	4	5	6	7	8
Euclidean	8.1	10.3	11.2	10.9	11.5	10.6	12.6	8.1	29.4	4.9	9.4	6.9	6.2	7.9	4.9	11.8
Chebyshev	8.4	9.6	6.8	10.6	13.3	12.2	11.4	8.7	29.4	5.6	9.3	5.6	4.9	11	8	5.6
City block	8.8	11.2	13.7	9	10.6	8.2	10.7	9.6	20	6.2	11.2	8.1	6.8	11	6.1	16.1
Cosine	12.8	6.8	10.9	9.7	11.2	7.6	12.9	7.4	15.6	5	8.7	6.9	7.5	4.9	8.6	13

Faulted

	Parallel					Non-parallel				
Fault size (mm)	0.25	0.5	0.75	1	1.5	0.25	0.5	0.75	1	1.5
Inner race fault										
Euclidean	59.1	86.4	69	67.3	72.1	41	49.3	40.6	47.2	45.1
Chebyshev	56.1	84.7	59.4	52.2	59.4	47.2	49.4	43.8	45.3	46.3
City block	58.7	85.2	73.2	70	72.8	35.4	43.8	40.6	46.6	41.4
Cosine	39.8	41.3	36	37.6	39.4	38.5	58.8	31.3	25.5	21.6
Outer race fault										
Euclidean	59.8	84	78.9	78.3	73.3	52.5	85.4	73.1	81.3	57.5
Chebyshev	60.9	84.3	80.8	79.9	72.6	55	84.2	75.6	79.5	71.2
City block	57.6	82.2	77.5	76.9	73.1	41.9	88.4	54.3	81.4	49.4
Cosine	35.1	50.4	44.3	47.1	38.3	54.4	81.7	75.6	77	77.5
Rolling-element fault										
Euclidean	8.7	11.4	11.7	8.7	14.8	9.4	7.5	11.8	6.2	27.3
Chebyshev	9.4	9.3	12.3	8.7	14.2	11.3	11.3	11.8	9.3	24.2
City block	9.6	13.2	12.3	9.6	16.5	11.3	8.1	13.7	9.9	26.7
Cosine	11.8	11.7	15	16	15	1.2	4.4	4.3	3.7	24.2

Table III.
Statistical feature results

Healthy

	Parallel								Non-parallel							
Test number	1	2	3	4	5	6	7	8	1	2	3	4	5	6	7	8
Euclidean	13.8	6.5	5.2	10.0	2.2	0.9	15.0	9.9	10.0	10.6	7.5	7.5	14.3	11.0	14.7	3.1
Chebyshev	14.4	7.8	9.9	8.7	5.0	1.5	13.5	6.5	12.5	10.6	5.6	8.1	13.7	7.9	17.2	1.8
City block	15	6.5	7.5	16.2	0.6	0.3	19.3	11.5	9.4	11.8	6.8	8.1	14.3	11.0	14.7	3.7
Cosine	6.6	1.8	11.5	14.0	10.9	8.2	23.3	7.1	14.4	8.7	8.1	7.5	12.4	8.5	11.0	2.5

Faulted

	Parallel					Non-parallel				
Fault size (mm)	0.25	0.5	0.75	1	1.5	0.25	0.5	0.75	1	1.5
Inner race fault										
Euclidean	77.7	87.2	66.6	68.5	70.5	36.7	75.6	35.6	12.4	42.6
Chebyshev	80.2	89.5	74.6	72.3	79.0	60.2	81.9	55.6	37.9	58.0
City block	75.7	86.3	65.1	67.1	65.0	35.4	65.0	23.8	6.8	20.4
Cosine	48.5	38.3	50.2	50.6	37.4	7.4	8.1	11.3	2.5	9.9
Outer race fault										
Euclidean	55.1	73.4	57.7	55.4	68.3	7.5	35.4	10.6	14.3	6.3
Chebyshev	53.7	73.1	58.8	56.1	65.4	17.5	72.6	25.0	39.8	25.0
City block	52.1	70.0	55.4	54.4	64.8	10.0	7.3	5.6	10.6	6.9
Cosine	42.6	39.8	46.4	39.5	50.2	8.1	3.0	7.5	8.1	5.6
Rolling-element fault										
Euclidean	30.1	38.3	24.5	24.7	38.9	5.6	7.5	8.1	13.7	14.9
Chebyshev	29.4	36.3	19.7	22.4	42.8	6.9	9.4	7.5	11.8	37.3
City block	32.2	36.8	24.1	24.6	36.3	5.6	7.5	8.1	13.0	13.0
Cosine	10.4	14.8	7.0	15.7	29.4	5.0	7.5	8.1	9.9	9.9

Table IV.
Autoregressive results

Moreover, the AR features using the parallel approach is this only method here that produces a significant disparity between the healthy tests and the rolling-element fault data. Similar to the statistics features, Euclidean and Chebyshev are the two best distance metrics while the cosine is again the worst.

4.1.3 Envelope analysis features. The envelope analysis features are shown in Table V to provide the best classification results for both the inner and outer race faults. However, like

Healthy

	Parallel								Non-parallel							
Test number	1	2	3	4	5	6	7	8	1	2	3	4	5	6	7	8
Euclidean	5.0	6.8	11.8	3.1	9.3	7.3	13.5	11.8	7.5	7.5	9.9	13.8	10.6	13.4	10.4	10.6
Chebyshev	6.3	6.2	10.6	3.8	8.6	6.7	13.5	11.2	11.3	8.1	8.7	10.0	11.8	11.6	8.0	11.8
City block	5.6	8.1	9.9	3.1	9.3	4.9	14.1	11.8	10.6	7.5	9.9	16.3	12.4	14.0	7.4	11.2

Faulted

	Parallel					Non-parallel				
Fault size (mm)	0.25	0.5	0.75	1	1.5	0.25	0.5	0.75	1	1.5
Inner										
Euclidean	82.1	84.7	83.5	81.2	83.3	67.3	87.6	73.3	79.1	82.1
Chebyshev	82.7	83.2	82.9	80.9	83.3	62.3	87.6	73.9	75.5	83.9
City block	79.0	84.4	83.2	81.5	83.6	69.1	88.2	73.9	78.5	79.6
Outer										
Euclidean	74.7	77.8	80.0	79.1	83.5	16.9	30.6	31.3	12.5	27.3
Chebyshev	74.7	77.8	77.8	78.5	82.2	15.0	23.1	27.5	13.8	12.4
City block	74.1	76.5	79.7	77.9	82.5	18.8	29.4	37.5	13.1	32.9
Rolling-element										
Euclidean	10.6	8.1	10.9	8.7	32.7	19.3	10.0	20.0	10.7	11.9
Chebyshev	10.0	7.2	10.6	10.3	34.6	20.5	10.0	21.3	8.7	11.3
City block	10.6	8.1	9.7	8.4	31.1	19.3	12.5	17.5	11.8	12.5

Table V.
Envelope analysis results

the statistics features, they do not produce a significant result for the rolling-element fault in either the parallel or non-parallel cases. Like the other features, the parallel method yields increased performance for the inner and outer race faults. Specifically, it can be seen that the outer race fault classification results increase drastically when using the parallel approach. The Euclidean and Chebyshev distances again preform the best in most cases.

4.2 Classification results with respect to speed/load

In this section, results for healthy tests and one specific fault type are broken down into nine different categories, each category containing results from different steady state levels of speed and load. The fault type analyzed is 1.5 mm outer race fault and the analysis method used is the parallel method with AR and envelope analysis features along with Euclidean distance.

The results in Table VI show that the parallel method preforms excellently for both 400 and 600 rpm cases. However, the results for the 200 rpm sections are not sufficient. This could be due to a relatively weak fault signature at slow speeds creating a low signal to noise ratio at 200 rpm or it could be a result of the change in features at slow speeds getting lost in the variation due to the non-stationary nature of the machine. The load appears to have minimal effect on the systems performance. Table VI also shows the results for the same tests when each of the subcategories is analyzed separately (separate normalization and thresholds for each category). It shows that while the 200 rpm results are still lower than the faster speeds, they increase significantly from the earlier results. This likely means that the decreased performance for 200 rpm is a result of both factors mentioned earlier.

Table VII shows the same type of results but with the envelope analysis feature vector instead of AR. These results also show decreased performance for the 200 rpm sections.

	Faulted			Healthy		
Classification results with respect to speed and load						
Speed (rpm)	200	400	600	200	400	600
Low load	10.5	100	100	41.1	0	15.7
Medium load	26.0	98.6	100	4.3	3.6	0
High load	52.2	94.2	100	17.4	36.5	6.1
Classification results with respect to speed and load when analyzed separately						
Speed (rpm)	200	400	600	200	400	600
Low load	68.4	100	100	9.8	7.3	8.9
Medium load	82.6	100	100	8.6	9.5	7.0
High load	95.6	100	100	8.6	9.6	9.1

Table VI. Autoregressive results with respect to operating conditions

	Faulted			Healthy		
Classification results with respect to speed and load						
Speed (rpm)	200	400	600	200	400	600
Low load	63.1	86.7	100	13.4	1.8	6.8
Medium load	52.2	83.6	91.6	8.3	4.8	1.2
High load	60.9	78.8	86.6	13.6	0	11.3
Classification results with respect to speed and load when analyzed separately						
Speed (rpm)	200	400	600	200	400	600
Low load	68.4	100	100	9.6	9.4	7.9
Medium load	60.8	99.3	98.8	8.3	9.0	9.5
High load	69.5	98.1	97.6	9.1	9.6	8.8

Table VII. Envelope analysis results with respect to operating conditions

However, the increase in performance for the 200 rpm section when analyzing them separately is not as drastic as with the AR features. This indicates that the Envelope analysis features are not as sensitive to the speed and load changes.

5. Conclusions

By utilizing the information that can be gained from mechanical systems that operate in a parallel manner, the accuracy of a fault detections system can be increased. Moreover, the proposed method was able to detect inner and outer race faults with improved accuracy when operating in parallel. Using this method, it was found that while envelope analysis yielded the best results for the inner and outer race faults, the AR features were the only set able to produce significant results for all three fault types considered here (inner race, outer race and rolling-element). It was also shown that when using the proposed method both Euclidean and Chebyshev distances preform consistently well for all cases while city block and cosine distances did not. The proposed method was able to detect faults during all operating states, however, the performance was severely decreased for the low speed sections. The key implication of this research is that where there is a parallel arrangement between mechanical components, it is possible to achieve significant improvements in fault detection accuracy if the two subsystems are analyzed together rather than as individual systems. While this work focused on two subsystems it is possible to apply this to any number of parallel subsystems. It would be expected that increasing the number of subsystems would aid in the detection and isolation of faults due to the increased degree of redundancy. However, this would come at the cost of increasing the number of residual calculations necessary.

References

Abboud, D., Antoni, J., Eltabach, M. and Sieg-Zieba, S. (2015), "Angle\time cyclostationarity for the analysis of rolling element bearing vibrations", *Measurement: Journal of the International Measurement Confederation*, Vol. 75, pp. 29-39.

Abboud, D., Antoni, J., Sieg-Zieba, S. and Eltabach, M. (2017), "Envelope analysis of rotating machine vibrations in variable speed conditions: a comprehensive treatment", *Mechanical Systems and Signal Processing*, Vol. 84, pp. 200-226.

Assaad, B., Eltabach, M. and Antoni, J. (2014), "Vibration based condition monitoring of a multistage epicyclic gearbox in lifting cranes", *Mechanical Systems and Signal Processing*, Vol. 42 Nos 1-2, pp. 351-367.

Barszcz, T. and Sawalhi, N. (2012), "Fault detection enhancement in rolling element bearings using the minimum entropy deconvolution", *Archives of Acoustics*, Vol. 37 No. 2, pp. 131-141.

Cong, F., Chen, J. and Dong, G. (2012), "Spectral kurtosis based on AR model for fault diagnosis and condition monitoring of rolling bearing", *Journal of Mechanical Science and Technology*, Vol. 26 No. 2, pp. 301-306.

Figueiredo, E., Figueiras, J., Park, G., Farrar, C.R. and Worden, K. (2011), "Influence of the autoregressive model order on damage detection", *Computer-Aided Civil and Infrastructure Engineering*, Vol. 26 No. 3, pp. 225-238.

Gertler, J. (1997), "Fault detection and isolation using parity relations", *Control Engineering Practice*, Vol. 5 No. 5, pp. 653-661.

Gor, M.M., Pathak, P.M., Samantaray, A.K., Yang, J.-M. and Kwak, S.W. (2018), "Fault accommodation in compliant quadruped robot through a moving appendage mechanism", *Mechanism and Machine Theory*, Vol. 121, pp. 228-244.

Goreczka, S. and Strackeljan, J. (2012), "Comparison of one-class classifiers for condition monitoring of rolling bearings in non-stationary operations", *9th International Conference on Condition Monitoring and Machinery Failure Prevention Technologies*, Vol. 2, pp. 683-695.

Helm, D. and Timusk, M. (2017), "Using residual analysis for the detection of faults in unsteadily operating rolling element bearings", *First World Congress on Condition Monitoring*, British Institute of Non-Destructive Testing, London, pp. 1465-1475.

Helm, D.M., Rose, A.M. and Timusk, M. (2016), "Condition monitoring of rolling-element bearings in parallel operating belt drive systems", *International Journal of COMADEM*, Vol. 19 No. 3, pp. 61-64.

Hoell, S. and Omenzetter, P. (2016), "Optimal selection of autoregressive model coefficients for early damage detectability with an application to wind turbine blades", *Mechanical Systems and Signal Processing*, Vols 70-71, pp. 557-577.

Isermann, R. (2006), "Fault-diagnosis systems: an introduction from fault detection to fault tolerance", *Fault-Diagnosis Systems: An Introduction from Fault Detection to Fault Tolerance*, Springer, Berlin and Heidelberg, pp. 1-475.

Isermann, R. and Ballé, P. (1997), "Trends in the application of model-based fault detection and diagnosis of technical processes", *Control Engineering Practice*, Vol. 5 No. 5, pp. 709-719.

Jiang, F., Zhu, Z., Li, W., Chen, G. and Zhou, G. (2014), "Robust condition monitoring and fault diagnosis of rolling element bearings using improved EEMD and statistical features", *Measurement Science and Technology*, Vol. 25 No. 2, pp. 1-14.

Kay, S.M. and Marple, S.L. Jr (1981), "Spectrum analysis – a modern perspective", *Proceedings of the IEEE*, Vol. 69 No. 11, pp. 1380-1419.

Law, L.-S., Kim, J.H., Liew, W.Y.H. and Lee, S.-K. (2012), "An approach based on wavelet packet decomposition and Hilbert-Huang transform (WPDHHT) for spindle bearings condition monitoring", *Mechanical Systems and Signal Processing*, Vol. 33, pp. 197-211.

McBain, J. and Timusk, M. (2009), "Fault detection in variable speed machinery: statistical parameterization", *Journal of Sound and Vibration*, Vol. 327 Nos 3-5, pp. 623-646.

McBain, J., Lakanen, G. and Timusk, M. (2013), "Vibration- and acoustic-emissions based novelty detection of fretted bearings", *Journal of Quality in Maintenance Engineering*, Vol. 19 No. 2, pp. 181-198.

McDonald, G.L., Zhao, Q. and Zuo, M.J. (2012), "Maximum correlated Kurtosis deconvolution and application on gear tooth chip fault detection", *Mechanical Systems and Signal Processing*, Vol. 33, pp. 237-255.

Medjaher, K., Samantaray, A.K., Bouamama, B.O. and Staroswiecki, M. (2006), "Supervision of an industrial steam generator. Part II: online implementation", *Control Engineering Practice*, Vol. 14 No. 1, pp. 85-96.

Prudhom, A., Antonino-Daviu, J., Razik, H. and Climente-Alarcon, V. (2017), "Time-frequency vibration analysis for the detection of motor damages caused by bearing currents", *Mechanical Systems and Signal Processing*, Vol. 84, pp. 747-762.

Randall, R.B. (2004a), "State of the art in monitoring rotating machinery – part 1", *Sound and Vibration*, Vol. 38 No. 3, pp. 14-21+13.

Randall, R.B. (2004b), "State of the art in monitoring rotating machinery – part 2", *Sound and Vibration*, Vol. 38 No. 5, pp. 10-17.

Randall, R.B. and Antoni, J. (2011), "Rolling element bearing diagnostics – A Tutorial", *Mechanical Systems and Signal Processing*, Vol. 25 No. 2, pp. 485-520.

Rose, A.M., Helm, D.M. and Timusk, M. (2016), "Fault detection of parallel hydraulic pumps in non-stationary operation", *International Journal of COMADEM*, Vol. 19 No. 3, pp. 55-59.

Samy, M. and Bassiuny, A.M. (2016), "Online bearing fault detection using linear prediction and nonlinear energy operator", *Proceedings of the IEEE International Conference on Electronics, Circuits, and Systems*, *March*, pp. 605-608.

Sawalhi, N., Randall, R.B. and Endo, H. (2007), "The enhancement of fault detection and diagnosis in rolling element bearings using minimum entropy deconvolution combined with spectral kurtosis", *Mechanical Systems and Signal Processing*, Vol. 21 No. 6, pp. 2616-2633.

Staroswiecki, M. and Comtet-Varga, G. (2001), "Analytical redundancy relations for fault detection and isolation in algebraic dynamic systems", *Automatica*, Vol. 37 No. 5, pp. 687-699.

Timusk, M., Lipsett, M. and Mechefske, C.K. (2008), "Fault detection using transient machine signals", *Mechanical Systems and Signal Processing*, Vol. 22 No. 7, pp. 1724-1749.

Uma Maheswari, R. and Umamaheswari, R. (2017), "Trends in non-stationary signal processing techniques applied to vibration analysis of wind turbine drive train – a contemporary survey", *Mechanical Systems and Signal Processing*, Vol. 85, pp. 296-311.

Wang, W. and Kanneg, D. (2009), "An integrated classifier for gear system monitoring", *Mechanical Systems and Signal Processing*, Vol. 23 No. 4, pp. 1298-1312.

Wang, X. and Makis, V. (2009), "Autoregressive model-based gear shaft fault diagnosis using the Kolmogorov-Smirnov test", *Journal of Sound and Vibration*, Vol. 327 Nos 3-5, pp. 413-423.

Wiggins, R. (1978), "Minimum entropy deconvolution", *Geophysics*, Vol. 16 Nos 1-2, pp. 21-35.

Willersrud, A., Blanke, M. and Imsland, L. (2015), "Incident detection and isolation in drilling using analytical redundancy relations", *Control Engineering Practice*, Vol. 41, pp. 1-12.

Zaretsky, E.V. (2013), "Rolling bearing life prediction, theory, and application", available at: ntrs.nasa.gov (accessed August 13, 2018).

Zhao, G. and Wang, Z. (2011), "Time-frequency analysis for non-stationary signal from mechanical measurement of bearing vibration", *International Journal of Modelling, Identification and Control*, Vol. 13 No. 3, pp. 190-194.

Zimroz, R., Bartelmus, W., Barszcz, T. and Urbanek, J. (2014), "Diagnostics of bearings in presence of strong operating conditions non-stationarity – a procedure of load-dependent features processing with application to wind turbine bearings", *Mechanical Systems and Signal Processing*, Vol. 46 No. 1, pp. 16-27.

Corresponding author
Markus Timusk can be contacted at: mtimusk@laurentian.ca